

# Photon statistics of a quantum emitter close to a lattice of plasmonic nanoparticles

F. Carreño,<sup>1</sup> V. Yannopapas,<sup>2</sup> M. A. Antón,<sup>1</sup> and E. Paspalakis<sup>3</sup>

<sup>1</sup>*Faculty of Optics and Optometry, University Complutense of Madrid, C/Arcos de Jalón 118, 28037 Madrid, Spain*

<sup>2</sup>*Department of Physics, National Technical University of Athens, 157 80 Athens, Greece*

<sup>3</sup>*Department of Materials Science, School of Natural Sciences, University of Patras, Patras 265 04, Greece*



(Received 18 December 2018; published 5 August 2019)

We study theoretically the statistics of photons generated by a quantum emitter located in the vicinity of a periodic plasmonic nanostructure. The presented formalism is based on a macroscopic QED formalism in conjunction with a density-matrix approach in order to obtain the second-order correlation function of the emitted photons accounting for the influence of the plasmonic environment. The metallic reservoir coupling is computed using Green's-function theory, which, for a periodic lattice of scatterers, is calculated by a multiple-scattering method. We show that the photon statistics and the antibunching of emitted photons depend very strongly on the orientation of the quantum emitter relative to the lattice, on the transition frequency of the emitter, on the intensity of the applied field, and on the geometrical parameters of the nanoparticles, such as the shell thickness.

DOI: [10.1103/PhysRevA.100.023802](https://doi.org/10.1103/PhysRevA.100.023802)

## I. INTRODUCTION

Localized surface plasmons, plasma oscillations occurring at the surface of finite metallic nanostructures, can alter drastically the spontaneous emission properties of nearby quantum emitters (QEs) [1,2]. A large number of theoretical works have shown that the spontaneous emission spectra [3–6] or the resonance fluorescence spectra and the corresponding statistical properties of emitted light [7–24] of QEs in the vicinity of plasmonic nanostructures, like metallic or metal-dielectric nanostructures, are dramatically different from the case where the QEs are placed in an isotropic dielectric or free-space vacuum. These findings are also supported by experimental studies [25–30]. The plasmonically modified resonance fluorescence and photon statistics may have various potential applications in nanophotonics and quantum technologies, such as in ultrasensitive sensing, in single-photon emission, and in the generation of entangled photons.

An important problem in quantum optics is the study of the second-order (intensity-intensity) correlation function of a two-level system driven by a coherent laser field which may lead to the creation of photon antibunching in resonance fluorescence and the transition from antibunching to bunching depending on the excitation conditions [31–34]. The latter was originally studied more than 40 years ago by Carmichael and Walls [35] and Kimble and Mandel [36]. Several experimental results have been presented with different types of QEs like atoms [37], ions [38], molecules [39,40], and quantum dots [41], and these effects are crucial for the creation of single-photon sources [42,43].

The behavior of the intensity-intensity correlation function of a single driven two-level QE has been studied in the vicinity of different plasmonic nanostructures, such as a metallic nanosphere [7–9,18,21], two metallic nanospheres [9,21,23], and a metallic nanostructure composed of four nanostrips [10]. It has been found that the spontaneous decay rate, as modified by the Purcell effect, and the change in the applied

electric field, which can be strongly affected near plasmonic nanostructures, lead to strong modification of the intensity-intensity correlation function.

Here, we study the photon statistics of a two-level QE placed in the vicinity of a periodic plasmonic nanostructure, namely, a two-dimensional (2D) lattice of metal-coated silica nanoparticles (also known as plasmonic nanoshells). The plasmonic nanostructure under study, due to its periodic nature, gives a distinctively different optical response than its basic element, i.e., a single metal-coated silica nanoparticle [44], and can lead to strong suppression of the decay rate of a nearby QE, as well as of the strongly anisotropic Purcell effect for an orthogonal QE's electric dipole directions [45–47]. By employing a density-matrix formalism for the QE and a multiple-scattering technique for the electromagnetic (EM) Green's tensor, we show that the second-order correlation function of photons stemming from the QE can be enormously modified by the presence of the plasmonic environment. The degree of modification of the photon statistics (relative to pure vacuum) depends on the orientation of the dipole moment of the quantum emitter relative to the lattice, as well as on the geometrical characteristics of the NPs. In particular, we show that under weak external driving, for a QE with its dipole moment being parallel to the plasmonic lattice, one can obtain a huge delay in the characteristic crossing time from antibunching to bunching. We also study the intensity-intensity correlation function under stronger external driving and illustrate the emergence of a rather counterintuitive phenomenon: under appropriate driving conditions (when the external Rabi frequency is fixed) a reduction or enlargement of the crossing time is obtained when the decay rates are decreased or increased with regard to its value in ordinary vacuum.

This paper is organized as follows. In Sec. II we present the theoretical part of the paper, starting with the method for the calculation of the EM Green's tensor, the spontaneous decay rates, and electric-field modifications next to the periodic

plasmonic nanostructure. We continue with a density-matrix approach for the calculation of the second-order correlation function of the emitted light from the QE. Then, in Sec. III we present the numerical results of the paper for different parameters of the plasmonic nanostructure and the applied electromagnetic field, as well as for different directions of the QE electric dipole moments. Finally, we summarize our results in Sec. IV.

## II. THEORY

### A. EM Green's tensor for a 2D periodic nanostructure

The classical EM Green's tensor is defined through the following equation:

$$\nabla \times \nabla \times \mathbf{G}(\mathbf{r}, \mathbf{r}'; \omega) - k^2 \mathbf{G}(\mathbf{r}, \mathbf{r}'; \omega) = \mathbf{1}_3 \cdot \delta(\mathbf{r} - \mathbf{r}'), \quad (1)$$

where  $k = \sqrt{\epsilon_d} \omega / c$  is the wave vector inside the material,  $\omega$  is the angular frequency of light,  $c$  is the vacuum light speed, and  $\mathbf{1}_3$  is the  $3 \times 3$  unit matrix.

We are interested in arrays of nanospheres with 2D periodicity. However, the presented formalism for the EM Green's tensor is more general and entails the case of scatterers of arbitrary shape [48]. The method employed here is an EM Green's tensor formalism based on a layer-multiple-scattering (LMS) method, which is based on an *ab initio* multiple-scattering theory, using a well-documented computer code [49]. The LMS method is ideally suited for the calculation of the transmission, reflection, and absorption coefficients of an EM wave incident on a composite slab consisting of a number of layers that can be either planes of nonoverlapping scatterers with the same 2D periodicity or homogeneous plates. For each plane of particles, the method calculates the full multipole expansion of the total multiply scattered wave field and deduces the corresponding transmission and reflection matrices in the plane-wave basis [50]. The transmission and reflection matrices of the composite slab are evaluated from those of the constituent layers. Having determined the transmission and reflection matrices via the LMS method, one can proceed to the calculation of the EM Green's tensor from [45,51]

$$G_{ii'}^{EE}(\mathbf{r}, \mathbf{r}'; \omega) = g_{ii'}^{EE}(\mathbf{r}, \mathbf{r}'; \omega) - \frac{i}{8\pi^2} \iint_{SBZ} d^2 \mathbf{k}_{\parallel} \sum_{\mathbf{g}} \frac{1}{c^2 \mathbf{K}_{\mathbf{g}^+}^+} \times v_{\mathbf{g} \mathbf{k}_{\parallel}; i}(\mathbf{r}) \exp(-i \mathbf{K}_{\mathbf{g}^+} \cdot \mathbf{r}) \hat{\mathbf{e}}_i(\mathbf{K}_{\mathbf{g}^+}), \quad (2)$$

with

$$v_{\mathbf{g} \mathbf{k}_{\parallel}; i}(\mathbf{r}) = \sum_{\mathbf{g}'} R_{\mathbf{g}'; \mathbf{g}}(\omega, \mathbf{k}_{\parallel}) \exp(-i \mathbf{K}_{\mathbf{g}'} \cdot \mathbf{r}) \hat{\mathbf{e}}_i(\mathbf{K}_{\mathbf{g}'}), \quad (3)$$

and

$$\mathbf{K}_{\mathbf{g}}^{\pm} = \{\mathbf{k}_{\parallel} + \mathbf{g}, \pm[q^2 - (\mathbf{k}_{\parallel} + \mathbf{g})^2]^{1/2}\}. \quad (4)$$

The vectors  $\mathbf{g}$  denote the reciprocal-lattice vectors corresponding to the 2D periodic lattice of the plane of scatterers, and  $\mathbf{k}_{\parallel}$  is the reduced wave vector which lies within the surface Brillouin zone associated with the reciprocal lattice [49]. When  $q^2 = \omega^2/c^2 < (\mathbf{k}_{\parallel} + \mathbf{g})^2$ ,  $\mathbf{K}_{\mathbf{g}}^{\pm}$  defines an evanescent wave. The term  $g_{ii'}^{EE}(\mathbf{r}, \mathbf{r}'; \omega)$  in Eq. (2) is the free-space Green's tensor, and  $\hat{\mathbf{e}}_i(\mathbf{K}_{\mathbf{g}}^{\pm})$  is the polar unit vector normal to  $\mathbf{K}_{\mathbf{g}}^{\pm}$ .  $R_{\mathbf{g}'; \mathbf{g}}(\omega, \mathbf{k}_{\parallel})$  is the reflection matrix which provides the

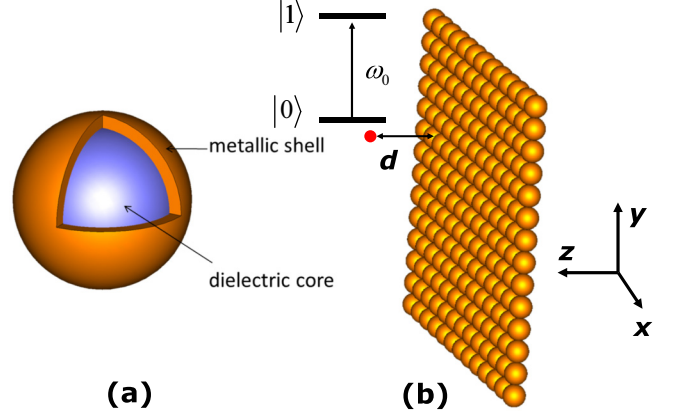


FIG. 1. (a) A metal-coated dielectric nanosphere and (b) a two-dimensional array of such spheres used in this work.

sum (over  $\mathbf{g}$ 's) of reflected beams generated by the incidence of the plane wave from the left of the plane of scatterers and is calculated via the LMS code [49]. We note that Eq. (2) is derived from the transverse part of the general classical-wave Green's tensor [51]. Also, in Eq. (2), the terms corresponding to *s*-polarized waves [those containing components with the azimuthal unit vector  $\hat{\mathbf{e}}_i(\mathbf{K}_{\mathbf{g}}^{\pm})$  normal to  $\mathbf{K}_{\mathbf{g}}^{\pm}$ ] have a small contribution to the decay rates and have been, therefore, neglected.

The plasmonic nanostructure considered in this work is a 2D array of touching metal-coated silica nanospheres [see Figs. 1(a) and 1(b)]. The dielectric function of the shell is provided by a Drude-type electric permittivity given by

$$\epsilon_m(\omega) = 1 - \frac{\omega_p^2}{\omega(\omega + i/\tau)}, \quad (5)$$

where  $\omega_p$  is the bulk plasma frequency and  $\tau$  is the relaxation time of the conduction-band electrons of the metal.

### B. Quantum light-matter interaction and the intensity-intensity correlation function

The QE is considered a two-level system with ground state  $|0\rangle$  and excited state  $|1\rangle$ , with  $\omega_0$  being the transition frequency. When describing the quantum light-matter interaction, we follow a medium-dependent quantization procedure to derive the equation of motion of populations and coherences of the system in a lossy, inhomogeneous environment [52,53].

We begin with the Hamiltonian of the coupled system, namely,

$$H = \hbar \omega_0 \sigma_z + \hbar \Omega (\sigma^+ e^{-i\omega_L t} + \sigma^- e^{+i\omega_L t}) + \hbar \int d^3 \mathbf{r} \int_0^\infty d\omega_k \omega_k \hat{\mathbf{f}}^\dagger(\mathbf{r}, \omega_k; t) \cdot \hat{\mathbf{f}}(\mathbf{r}, \omega_k; t) - \left[ \sigma^+ \int_0^\infty d\omega_k \mathbf{d} \cdot \mathbf{E}(\mathbf{r}_0, \omega_k) + \text{H.a.} \right], \quad (6)$$

where  $\sigma^\pm$  are the Pauli raising and lowering operators of the two-level system located at  $\mathbf{r}_0$ , and driven by an external field of angular frequency  $\omega_L$  and amplitude  $\mathbf{E}_0(\mathbf{r})$ . Also,  $\hat{\mathbf{f}}^\dagger$  ( $\hat{\mathbf{f}}$ ) stands for the bosonic continuum field creation (annihilation)

operator of the total electric-field operator. In writing Eq. (6) we have used an index scheme with continuous eigenfrequencies  $\omega_k$ , while  $\mathbf{d}$  stands for the dipole which is assumed to be real without loss of generality.

The effective Rabi frequency is determined through  $\Omega = \langle \mathbf{E}_{\text{driv}}(\mathbf{r}_0, \omega_L) \rangle \cdot \mathbf{d} / 2\hbar$ . Note that the pump field consists of the external pumping term plus the scattered field produced by the metallic nanostructure and reads

$$\mathbf{E}_{\text{driv}}(\mathbf{r}_0, \omega_L) = \mathbf{E}_0(\mathbf{r}_0) + \int_{\text{Vol}_{MNP}} d^3\mathbf{r}' \mathbf{G}(\mathbf{r}_0, \mathbf{r}', \omega_L) \times [\epsilon_m(\omega_L) - 1] \mathbf{E}_0(\mathbf{r}_0). \quad (7)$$

The spatial integration in Eq. (7) must be done over the volume of the nanostructure. In this way we can estimate that the effective Rabi frequency is  $\Omega = \Omega_0 \eta_{pl}^u$ , with  $\Omega_0 = \mathbf{E}_0 \cdot \mathbf{d} / (2\hbar)$  being the free-space Rabi frequency. Thus, the quantity  $\eta_{pl}^u$  can be considered an enhancement (screening) factor depending on whether the modulus is larger (lower) than unity, while  $u = x$  or  $u = z$  depending on whether the incident field oscillates along the  $X$  or  $Z$  axis, respectively. On the other hand, the field  $\mathbf{E}(\mathbf{r}_0, \omega_k)$  (excluding the external field) is obtained through [53]

$$\mathbf{E}(\mathbf{r}_0, \omega_k) = \frac{1}{\epsilon_0} \int d^3\mathbf{r}' \mathbf{G}(\mathbf{r}_0, \mathbf{r}', \omega_k) \cdot \sqrt{\frac{\hbar \epsilon_0}{\pi}} \text{Im}[\epsilon_m(\mathbf{r}', \omega_k)] \hat{\mathbf{f}}(\mathbf{r}', \omega_k). \quad (8)$$

In a frame rotating at the laser frequency  $\omega_L$  we can write the Hamiltonian in Eq. (6) as  $H = H_{\text{sys}} + H_{\text{rad}} + H_{\text{int}}$ , where the system, the bath, and the system-reservoir interaction terms are given as

$$\begin{aligned} H_{\text{sys}} &= \hbar(\omega_0 - \omega_L) \sigma_z + \hbar\Omega(\sigma^+ + \sigma^-) \\ H_{\text{rad}} &= \hbar \int d^3\mathbf{r} \int_0^\infty d\omega_k \omega_k \hat{\mathbf{f}}^\dagger(\mathbf{r}, \omega_k; t) \cdot \hat{\mathbf{f}}(\mathbf{r}, \omega_k; t), \\ H_{\text{int}} &= -\left[ \sigma^+ \int_0^\infty d\omega_k \mathbf{d} \cdot \mathbf{E}(\mathbf{r}_0, \omega_k) + \text{H.a.} \right], \end{aligned} \quad (9)$$

where we have used the unitary transformation  $U(t) = \exp[-iH_{\text{rad}}t/\hbar]$ , as we are interested in a regime where the external Rabi frequency  $\Omega_0$  is within the range of the free-space decay rate of the atomic system  $\Gamma_0$  and the field enhancement  $\eta_{pl}$  is close to unity, as shown below.

The transformed Hamiltonian reads  $\tilde{H} = U^\dagger(t) H U(t)$ . By taking the trace over the reservoir in the interaction picture, within the Born-Markov approximation to second order in interaction, and then by going back to the original picture, we obtain the following master equation:

$$i\hbar \frac{\partial}{\partial t} \rho = [H_{\text{sys}}, \rho] + \mathcal{L}\rho, \quad (10)$$

where  $\mathcal{L}\rho$  stands for the Liouvillian of the system interacting with the nanostructured reservoir, reading  $\mathcal{L}\rho = \frac{\Gamma}{2}(2\sigma^- \rho \sigma^- - \sigma^+ \sigma^- \rho - \rho \sigma^+ \sigma^-)$ .  $\Gamma$  is obtained through

$$\Gamma = \frac{\mu_0 \mu^2 \omega_0^2}{\hbar} \{ \hat{\mathbf{u}} \cdot \text{Im} \mathbf{G}(\mathbf{r}, \mathbf{r}; \omega_0) \cdot \hat{\mathbf{u}} \}, \quad (11)$$

with  $\hat{\mathbf{u}}$  being the unit vector in the direction of the dipole moment  $\mathbf{d}$ . In deriving the Liouvillian in Eq. (10) we have

considered the plasmonic reservoir to be at zero temperature, which in the optical range is quite adequate.

We are interested in the statistical properties of the light scattered by the QE in close proximity to the plasmonic nanostructure. This is done by evaluating the normalized second-order correlation function of the fluorescent signal emitted by the system [31–34], given by

$$g^{(2)}(\vec{r}, t, \vec{r}, t + \tau) = \frac{G^{(2)}(\vec{r}, t, \vec{r}, t + \tau)}{G^{(1)}(\vec{r}, t) G^{(1)}(\vec{r}, t + \tau)}. \quad (12)$$

The first- and second-order correlation functions appearing in Eq. (12) can be expressed in terms of the positive- and negative-frequency parts of the electric-field operators as

$$\begin{aligned} G^{(1)}(\vec{r}, t) &= \langle \vec{E}^-(\vec{r}, t) \vec{E}^+(\vec{r}, t) \rangle, \\ G^{(2)}(\vec{r}, t, \vec{r}, t + \tau) &= \langle \vec{E}^-(\vec{r}, t) \vec{E}^-(\vec{r}, t + \tau) \\ &\quad \times \vec{E}^+(\vec{r}, t + \tau) \vec{E}^+(\vec{r}, t) \rangle, \end{aligned} \quad (13)$$

while the negative-frequency part of the fluorescent field in the far-field zone ( $|\vec{r}| \gg c/\omega_0$ ) reads

$$\vec{E}^-(\vec{r}, t) = \frac{\omega_0^2}{c^2 |\vec{r}|} d\sigma_{10}(t - |\vec{r}|/c) \hat{\mathbf{u}} \quad (14)$$

and  $\vec{E}^+(t) = [\vec{E}^-(t)]^\dagger$ . We assume that the first- and second-order correlation functions leading to Eq. (12) are determined under stationary conditions by invoking the quantum regression theorem. In the particular case where the system is driven on resonance ( $\omega_L = \omega_0$ ) it can be shown that [31,32]

$$\begin{aligned} g^{(2)}(\vec{r}, t, \vec{r}, t + \tau) \\ = 1 - e^{-(3/4)\Gamma\tau} \left[ \cosh(\kappa\tau) + \frac{3\Gamma}{4\kappa} \sinh(\kappa\tau) \right], \end{aligned} \quad (15)$$

where  $\kappa = 1/2\sqrt{\Gamma^2/4 - 16\Omega^2}$ . In view of Eq. (15) we can devise the existence of a threshold at  $\Omega = \Gamma/8$  below which the solution monotonically approaches the steady-state value of unity; that is, the system remains in the antibunching regime. And for values above the threshold, the solution tends to oscillate, exhibiting dark periods, where the emission of a second photon is inhibited until the system recovers from the previous emission and can produce a subsequent photon. In what follows we will define “crossing time”  $\tau_c$  as the instant when the system makes the first transition from antibunching to bunching, when applicable. It is clear that the second-order correlation function  $g^{(2)}(\vec{r}, t, \vec{r}, t + \tau)$  and the crossing time  $\tau_c$  depend strongly on the nanostructured photonic environment in which the QE is embedded. Their behavior for the specific 2D plasmonic nanostructure will be presented in the following section.

### III. RESULTS AND DISCUSSION

Now we resort to numerical simulations for the properties of the system. As a first step we determine the decay rates of a dipole located a certain distance  $d$  from the periodic nanostructure. We will normalize the angular frequencies and distances using the plasma frequency  $\omega_p$  of the metallic part of the nanostructure. We note that although this frequency is different from the plasmon frequency of the periodic nanostructure, it is more convenient to use it for normalization.

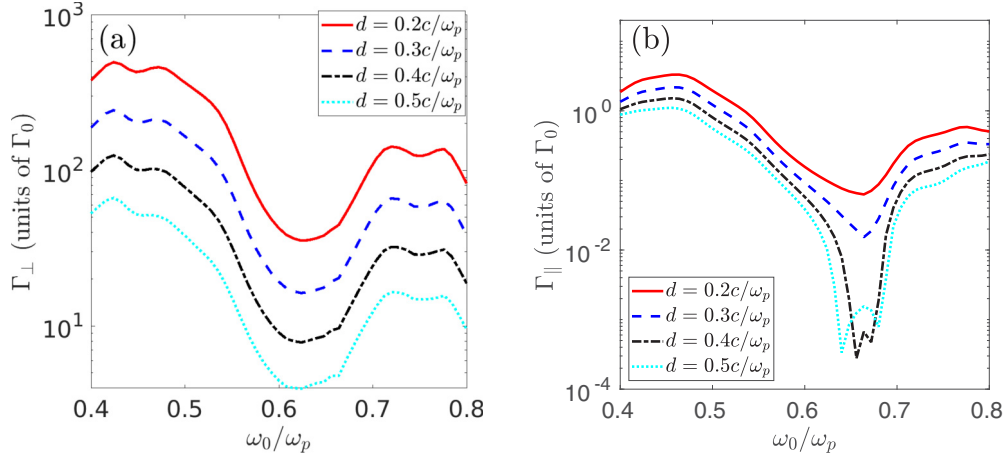


FIG. 2. Decay rate for a dipole which is oriented (a) normally and (b) parallel with respect to the plasmonic nanostructure as a function of the normalized emitter frequency  $\omega_0$  for various (normalized) distances  $d$  to the plasmonic nanostructure (with exact values of  $d$  shown in the inset).  $\Gamma_0$  is the decay rate in the vacuum.

A typical value for the plasma frequency for gold is  $\hbar\omega_p = 8.99$  eV. This also determines the length scale of the system as  $c/\omega_p \approx 22$  nm. The dielectric constant of  $\text{SiO}_2$  is taken as  $\epsilon = 2.1$ . In the calculations we have taken  $\tau^{-1} = 0.05\omega_p$ .

The lattice constant of the square lattice is  $a = 2c/\omega_p$ , and the sphere radius  $S = c/\omega_p$ , while the shell thickness  $d_{\text{shell}}$  (core radius  $S_c = S - d_{\text{shell}}$ ) is varied parametrically. The QE is placed at a distance  $d$  (in  $c/\omega_p$  units) from the nanostructure,

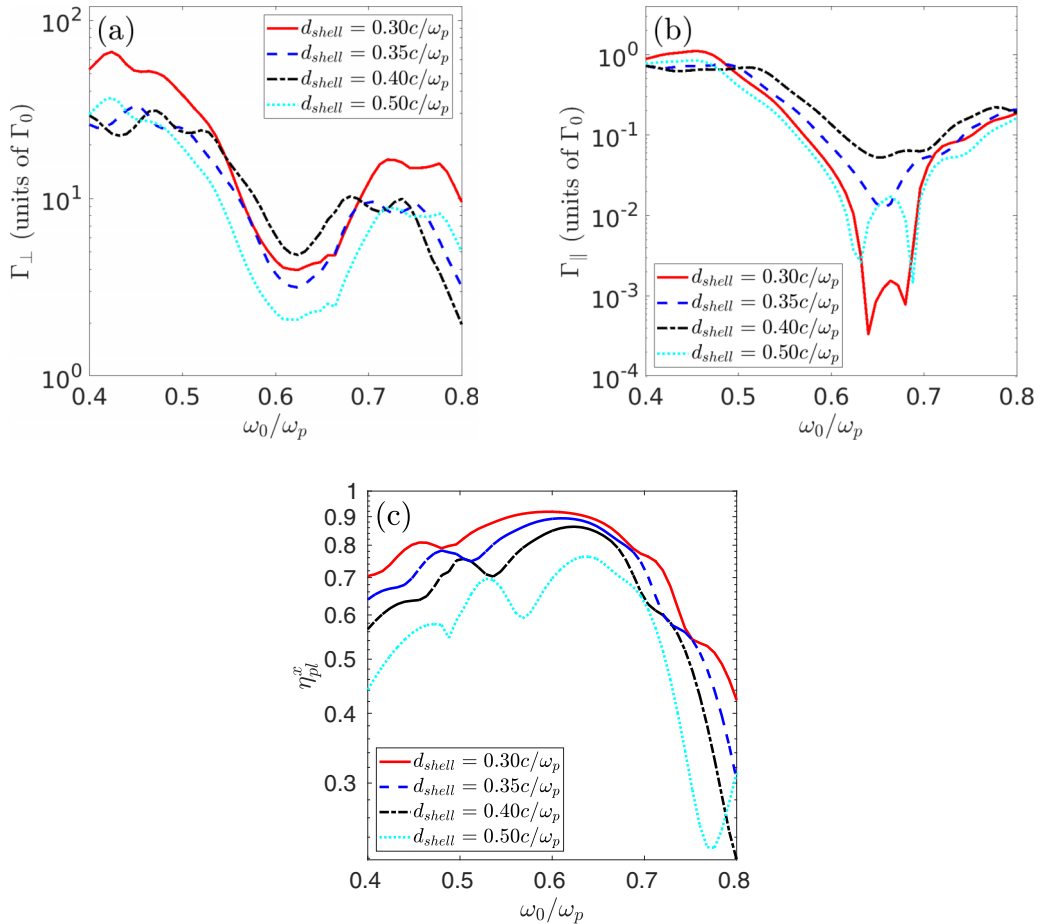


FIG. 3. Decay rate for a dipole which is oriented (a) normally and (b) parallel with respect to the plasmonic nanostructure as a function of the normalized emitter frequency  $\omega_0$  for various (normalized) thicknesses  $d_{\text{shell}}$  (with exact values of  $d_{\text{shell}}$  shown in the inset).  $\Gamma_0$  is the decay rate in the vacuum, and the emitter is placed at a distance  $d = 0.5c/\omega_p$  from the lattice. (c) Field enhancement factor  $\eta_{pl}^x$  as a function of the normalized emitter frequency  $\omega_0$  for various (normalized) thicknesses  $d_{\text{shell}}$ .

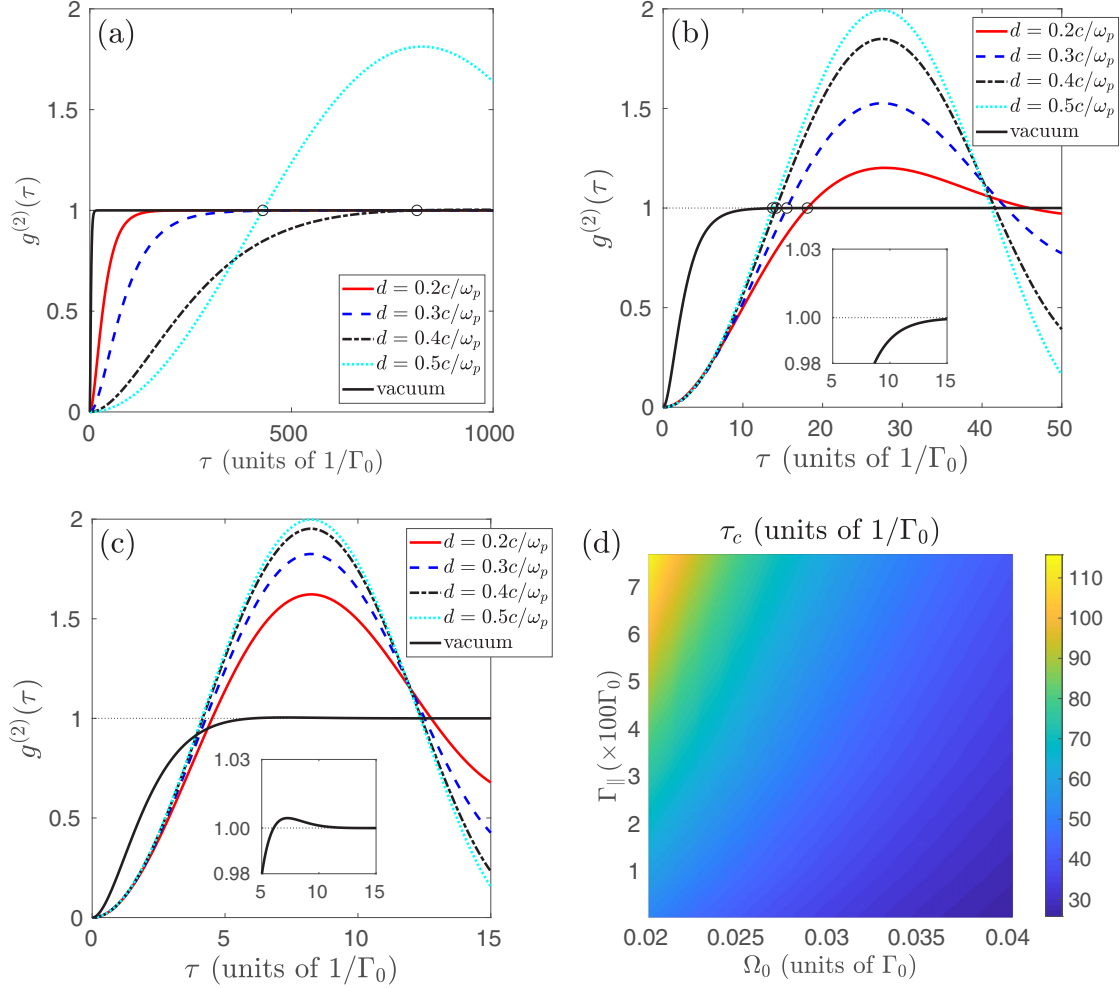


FIG. 4. Second-order correlation function of the emitted photons from a QE whose dipole moment is parallel to the nanostructure at different distances  $d$  from the lattice for a QE with transition frequency  $\omega_0 = 0.64\omega_p$ :  $d = 0.2c/\omega_p$  (red solid curve),  $d = 0.3c/\omega_p$  (blue dashed curve),  $d = 0.4c/\omega_p$  (black dash-dotted curve),  $d = 0.5c/\omega_p$  (cyan dotted curve). The solid black curve corresponds to the case without the 2D lattice. (a)  $\Omega_0 = 0.0025\Gamma_0$ , (b)  $\Omega_0 = 0.075\Gamma_0$ , and (c)  $\Omega_0 = 0.25\Gamma_0$ . (d) Crossing time  $\tau_c$  from antibunching to bunching as a function of the decay rate  $\Gamma_{\parallel}$  and the free-space Rabi frequency  $\Omega_0$ .

while its dipole moment may be oriented parallel or normal to the 2D lattice of nanoparticles.

Figure 2 shows the decay rates for a QE versus the transition frequency  $\omega_0$  in units of  $\omega_p$  for the cases where the dipole moment is oriented perpendicular ( $\Gamma_{\perp}$ ) and parallel ( $\Gamma_{\parallel}$ ) to the 2D lattice of nanoparticles (note that the decay rates are expressed in units of  $\Gamma_0$ , with  $\Gamma_0$  being the decay rate of the QE in the absence of the nanostructure). The reported calculation is based on Eq. (11). Here, we find that for a dipole oriented along the Z axis [see Fig. 2(a)] the decay rate exhibits a large enhancement (up to a 200-fold increase) at certain frequency values of  $\omega_0$ . As for the case where the dipole is oriented perpendicular to the Z axis, the decay rates are strongly reduced (up to a 20 000-fold decrease). This strong anisotropy of the decay rates will modify the photon statistics produced by the QE, as we will show below.

An additional degree of freedom to tailor the effect of the nanostructure on the QE is the selection of different designs for the individual nanoparticles which form the 2D nanostructure. The dependence of the decay rate on gold shell thickness  $d_{\text{shell}}$  of the nanoparticles comprising the lattice is

shown in Figs. 3(a) and 3(b). These two plots are derived for the same distance,  $d = 0.5c/\omega_p$ , between the QE and the 2D lattice. We observe that the degree of dependence on the shell thickness is not the same for the two types of dipole orientations (parallel and perpendicular).

In addition, we have calculated the field enhancement factor  $\eta_{pl}^x$  for the two different dipole orientations, as shown in Fig. 3(c). Namely, we observe that the field enhancement is less than unity, indicating a screening effect of the nanostructure on the applied EM field. It is worth mentioning that the numerical simulations reveal that the values of  $\eta_{pl}^x$  do not depend on the distance  $d$  since the electric field, at such distances, consists exclusively of far-field components of the EM field (propagating waves) and, as such, it does change with distance, as is the case for the near-field components (evanescent waves).

Figures 4(a)–4(c) present the time evolution of the intensity-intensity correlation of the emitted photons for several distances between the QE and the nanostructure, as well as for the QE in vacuum. The transition frequency of the QE is taken to be  $\omega_0 = 0.64\omega_p$ , which is in the region where the



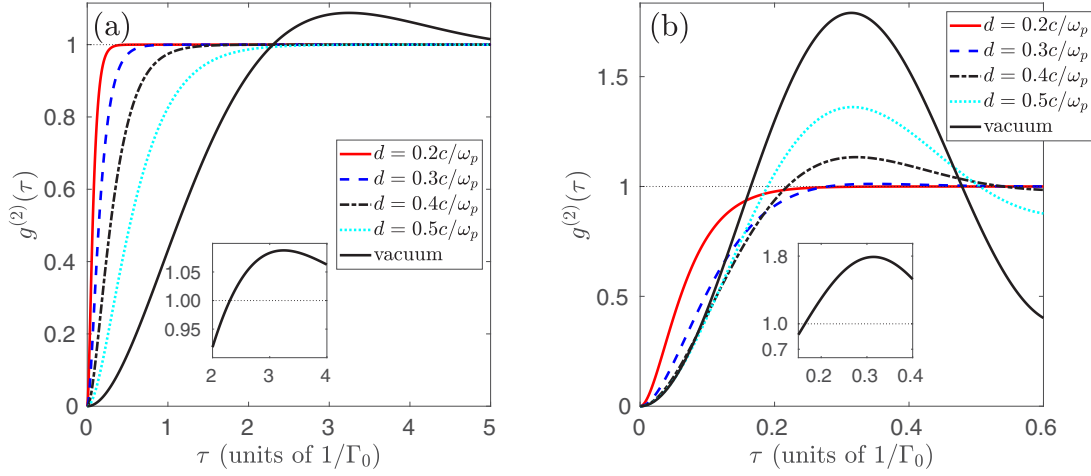


FIG. 5. Second-order correlation function of the emitted photons from a QE whose dipole moment is perpendicular to the nanostructure for different distances  $d$  from the lattice for a QE with transition frequency  $\omega_0 = 0.64\omega_p$ :  $d = 0.2c/\omega_p$  (red solid curve),  $d = 0.3c/\omega_p$  (blue dashed curve),  $d = 0.4c/\omega_p$  (black dash-dotted curve),  $d = 0.5c/\omega_p$  (cyan dotted curve). The solid black curve corresponds to the case without the 2D lattice. (a)  $\Omega_0 = 0.5\Gamma_0$  and (b)  $\Omega_0 = 5.0\Gamma_0$ .

decay rate  $\Gamma_{\parallel}$  exhibits strong suppression with respect to the free-space case. The Rabi frequencies used to produce these plots differ markedly: in Fig. 4(a), we have used a very small free-space Rabi frequency, so that the system remains in the antibunching regime when the QE is isolated. We observe that the solid and dashed curves show a similar behavior, whereas for the other two cases, the dash-dotted and dotted curves, we obtain large values for the crossing time, i.e.,  $\tau_c \approx 810/\Gamma_0$  and  $\tau_c \approx 430/\Gamma_0$ , respectively. These two values of  $\tau_c$  are depicted as open circles in Fig. 4(a). Even more dramatic results have been found from the study of the fluorescent field produced by QEs located close to different metallic nanostructures due to stronger suppression of the decay rates [9,21].

A small increment of the free-space Rabi frequency  $\Omega_0$  can produce dramatic changes for all the distances, as shown in Fig. 4(b). At the same time, the QE remains in the antibunching regime for the free-space case [see the inset in Fig. 4(b)]. In the presence of the nanostructure the situation is strongly altered compared to the QE in ordinary vacuum and, in spite of the extremely low value of  $\Omega_0$ , the hybrid system still exhibits Rabi oscillations. The origin of this behavior relies on the strong reduction of the decay rate, in which case the system reaches the threshold of oscillations, as discussed after Eq. (15). In the free-space case,  $\kappa$  remains real, and the system remains in the antibunching regime. Note that the crossing time  $\tau_c$  depends on the distance  $d$  between the QE and the nanostructure. The case presented in Fig. 4(c) is calculated by setting  $\Omega_0$  in the range above the threshold for the vacuum case [see the inset in Fig. 4(c)]. Here, we can readily observe that the effect of the nanostructure is to accelerate the transition to the bunching regime; that is, the value of  $\tau_c$  is shortened compared to the free-space case. For the case considered in Fig. 4(c), the crossing time  $\tau_c$  depends weakly on the distance  $d$ .

The time instant when the system exits the antibunching regime for the first time ( $\tau_c$ ) can be easily determined through numerical methods following Eq. (15). The dependence of this crossing time  $\tau_c$  on both the decay rate  $\Gamma_{\parallel}$  and the

free-space Rabi frequency  $\Omega_0$  is presented in Fig. 4(d). Here, the values of  $\Omega_0$  have been parametrically varied within the weak-driving limit, which is responsible for the large values of  $\tau_c$ , and delays the emission of a second photon after the first one is detected at  $\tau = 0$ .

Next, we study the case when the dipole moment of the QE is perpendicular to the 2D lattice. We have kept the transition frequency of the QE constant at  $\omega_0 = 0.64\omega_p$  as in the previous case. The results are presented in Fig. 5 for two values of the free-space Rabi frequency. Here, it is worth noting that the values of  $\Omega_0$  have been enhanced in comparison to the ones used to produce Fig. 4 so as to maintain the system either below or above the threshold condition for obtaining Rabi oscillations. As for the case depicted in Fig. 5(a), we observe the complete inhibition of a second photon emission when the QE is in the presence of the nanostructure for all the distances  $d$  considered. An increase of  $\Omega_0$  by an order of magnitude results in the curves depicted in Fig. 5(b). Here, the main effect of the nanostructure is to delay the transition to the bunching regime with respect to the value of  $\tau_c$  achieved in vacuum. This is in clear contrast to the results depicted in Fig. 4(c). The curves presented in Figs. 4(c) and 5(b) are counterintuitive in the sense that we obtain a reduction (enhancement) of the crossing time when the decay rates are decreased (increased) with respect to the values in ordinary vacuum.

Figures 6(a)–6(c) present the time evolution of the intensity-intensity correlation of the emitted photons for different shell thicknesses  $d_{\text{shell}}$  and a fixed distance from the QE to the 2D lattice (in comparison with the QE being in vacuum). In this case the transition frequency of the QE was selected to be  $\omega_0 = 0.568\omega_p$ , while we have taken various values for the free-space Rabi frequency. For the smallest value of  $\Omega_0$  we present the curves in Fig. 6(a). We observe that the values of the crossing time vary from  $\approx 75/\Gamma_0$  for the solid curve to  $\approx 250/\Gamma_0$  for the dashed curve. In this regime of low driving the isolated QE remains in the antibunching regime. In the case of the intermediate value of  $\Omega_0$  used to

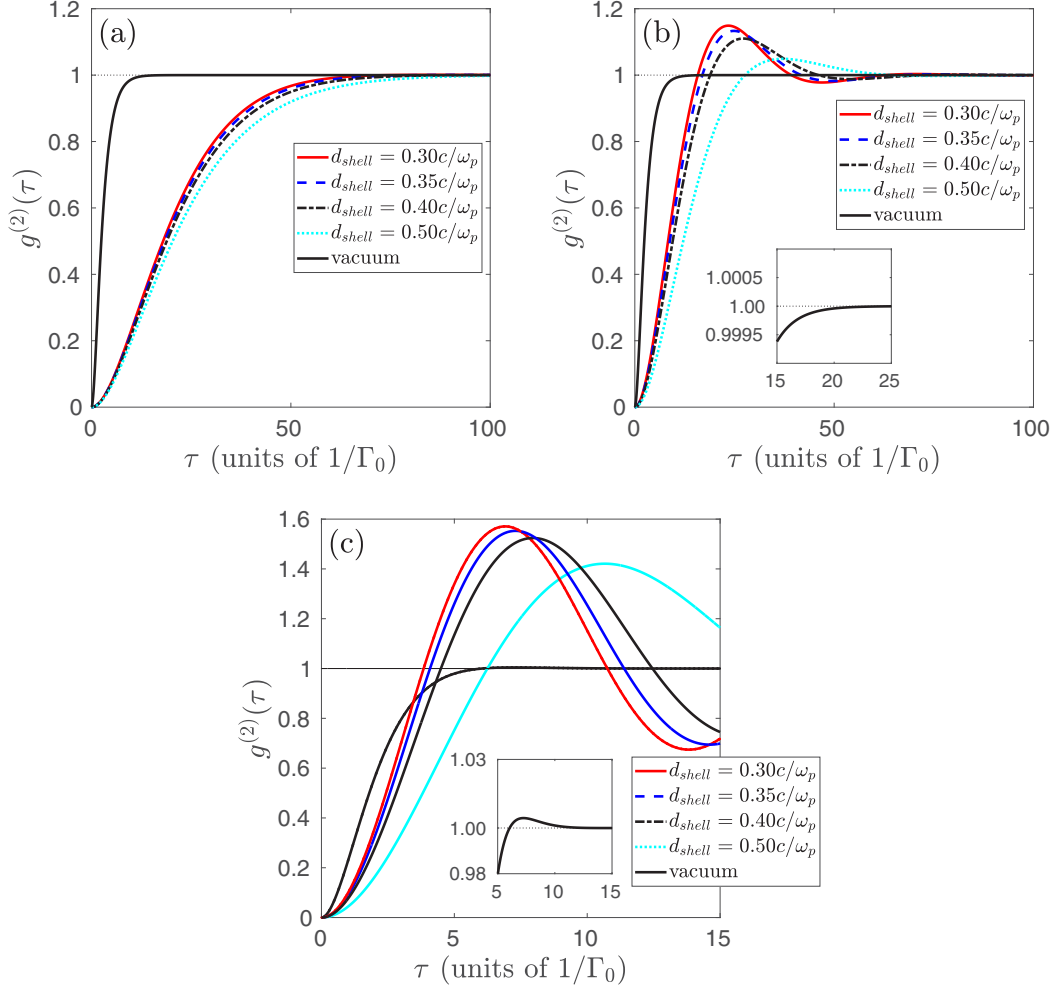


FIG. 6. Second-order correlation function of the emitted photons from a QE whose dipole moment is parallel to the nanostructure at a fixed distance  $d = 0.5c/\omega_p$  from the lattice and different values of the shell thickness for a QE with transition frequency  $\omega_0 = 0.568\omega_p$ :  $d_{\text{shell}} = 0.30c/\omega_p$  (red solid curve),  $d_{\text{shell}} = 0.35c/\omega_p$  (blue dashed curve),  $d_{\text{shell}} = 0.40c/\omega_p$  (black dash-dotted curve),  $d_{\text{shell}} = 0.50c/\omega_p$  (cyan dotted curve). The solid black curve corresponds to the case without the 2D lattice. (a)  $\Omega_0 = 0.025\Gamma_0$ , (b)  $\Omega_0 = 0.075\Gamma_0$ , and (c)  $\Omega_0 = 0.25\Gamma_0$ .

produce Fig. 6(b) we recover a result similar to the one found in Fig. 4(b). However, it should be noted that the values of  $\tau_c$  obtained for this QE differ from the previous ones. A similar trend is observed in Fig. 6(c), where the different curves grow apart from each other. The same holds for the period of the Rabi oscillations (related to  $1/\kappa$ ) as a consequence of the combined effect of the strong modifications of the decay rates and the field enhancement  $\eta_{pl}^x$ . Evidently, the time evolution of the intensity-intensity correlation may be strongly modified with the shell thickness, providing an additional degree of tunability for the statistics of the emitted photons.

#### IV. CONCLUSIONS

We have studied theoretically the photon statistics of light emitted by a QE in the vicinity of a two-dimensional array of metal-coated silica nanospheres. Namely, we have employed a macroscopic QED formalism along with a density-matrix approach in order to obtain the second-order correlation functions of the photons generated by the QE modified by the presence of an external photonic bath. The photonic

bath was simulated as that of a 2D square lattice of gold-coated silica spheres (gold nanoshells) via an electromagnetic Green's tensor. We have found, in particular, that the photon statistics are dramatically modified by the lattice of nanoparticles. In addition, we have shown that the crossing time from antibunching to bunching depends very strongly on the orientation of the quantum emitter relative to the lattice, on the transition frequency of the emitter, on the intensity of the applied electric field, and on the geometrical parameters of the nanoparticles. In particular, we have shown that for a weakly driven QE with its dipole moment being parallel to the plasmonic lattice, the characteristic crossing time can increase by two orders of magnitude relative to the case of the free-space vacuum. Under stronger external driving it was also shown that under appropriate driving conditions (when the external Rabi frequency is fixed), a reduction or enhancement of the crossing time is observed when the decay rates are decreased or increased with respect to their values in ordinary vacuum. Finally, we have also shown that the thickness of the plasmonic nanoshells can act as another control parameter of the photon statistics.

## ACKNOWLEDGMENTS

F.C. and M.A.A. acknowledge funding through projects PR41/17-21033 (UCM-Banco de Santander) and FIS2017-

87360-P (MICINN). V.Y. and E.P. acknowledge partial support from COST Action MP1403 Nanoscale Quantum Optics, supported by COST (European Cooperation in Science and Technology).

- 
- [1] M. S. Tame, K. R. McEnery, S. K. Ozdemir, J. Lee, S. A. Maier, and M. S. Kim, *Nat. Phys.* **9**, 329 (2013).
  - [2] F. Marquier, C. Sauvan, and J.-J. Greffet, *ACS Photonics* **4**, 2091 (2017).
  - [3] S. Evangelou, V. Yannopapas, and E. Paspalakis, *Phys. Rev. A* **83**, 023819 (2011).
  - [4] Y. Gu, L. Wang, P. Ren, J.-X. Zhang, T.-C. Zhang, O. J. F. Martin, and Q.-H. Gong, *Nano Lett.* **12**, 2488 (2012).
  - [5] C. Van Vlack, P. T. Kristensen, and S. Hughes, *Phys. Rev. B* **85**, 075303 (2012).
  - [6] J. Hakami, L. Wang, and M. S. Zubairy, *Phys. Rev. A* **89**, 053835 (2014).
  - [7] A. Ridolfo, O. Di Stefano, N. Fina, R. Saija, and S. Savasta, *Phys. Rev. Lett.* **105**, 263601 (2010).
  - [8] E. Waks and D. Sridharan, *Phys. Rev. A* **82**, 043845 (2010).
  - [9] R. Marty, A. Arbouet, V. Paillard, C. Girard, and G. Colas des Francs, *Phys. Rev. B* **82**, 081403(R) (2010).
  - [10] Y. Gu, L. Huang, O. J. F. Martin, and Q. Gong, *Phys. Rev. B* **81**, 193103 (2010).
  - [11] C. Sanchez-Munoz, A. Gonzalez-Tudela, and C. Tejedor, *Phys. Rev. B* **85**, 125301 (2012).
  - [12] F. Carreño, M. A. Antón, and F. Arrieta-Yáñez, *Phys. Rev. B* **88**, 195303 (2013).
  - [13] R. C. Ge, C. Van Vlack, P. Yao, J. F. Young, and S. Hughes, *Phys. Rev. B* **87**, 205425 (2013).
  - [14] S. M. Sadeghi, *Phys. Rev. A* **88**, 013831 (2013).
  - [15] K. Slowik, R. Filter, J. Straubel, F. Lederer, and C. Rockstuhl, *Phys. Rev. B* **88**, 195414 (2013).
  - [16] T. S. Theuerholz, A. Carmele, M. Richter, and A. Knorr, *Phys. Rev. B* **87**, 245313 (2013).
  - [17] D. Martín-Cano, H. R. Haakh, K. Murr, and M. Agio, *Phys. Rev. Lett.* **113**, 263605 (2014).
  - [18] M. A. Antón, F. Carreño, O. G. Calderón, S. Melle, and E. Cabrera, *J. Opt.* **18**, 025001 (2016).
  - [19] F. Carreño, M. A. Antón, V. Yannopapas, and E. Paspalakis, *Phys. Rev. A* **94**, 013834 (2016).
  - [20] F. Carreño, M. A. Antón, V. Yannopapas, and E. Paspalakis, *Phys. Rev. A* **95**, 043825 (2017).
  - [21] M. B. Harouni and M. R. N. Abadi, *Plasmonics* **12**, 1 (2017).
  - [22] E. Dumitrescu and B. Lawrie, *Phys. Rev. A* **96**, 053826 (2017).
  - [23] R. Sáez-Blázquez, J. Feist, A. I. Fernández-Domínguez, and F. J. García-Vidal, *Optica* **4**, 1363 (2017).
  - [24] D.-X. Zhao, *Phys. Rev. A* **98**, 033834 (2018).
  - [25] W. X. Wu, M. Gong, C. H. Dong, J. M. Cui, Y. Yang, F. W. Sun, G. C. Guo, and Z. F. Han, *Opt. Express* **18**, 6340 (2010).
  - [26] H. Naiki, S. Masuo, S. Machida, and A. Itaya, *J. Phys. Chem. C* **115**, 23299 (2011).
  - [27] S. Dey, Y. Zhou, X. Tian, J. A. Jenkins, O. Chen, S. Zou, and J. Zhao, *Nanoscale* **7**, 6851 (2015).
  - [28] S. Dey and J. Zhao, *J. Phys. Chem. Lett.* **7**, 2921 (2016).
  - [29] Y. Zhang, Q.-S. Meng, L. Zhang, Y. Luo, Y.-J. Yu, B. Yang, Y. Zhang, R. Esteban, J. Aizpurua, Y. Luo, J.-L. Yang, Z.-C. Dong, and J. G. Hou, *Nat. Commun.* **8**, 15225 (2017).
  - [30] M. A. Feldman, E. F. Dumitrescu, D. Bridges, M. F. Chisholm, R. B. Davidson, P. G. Evans, J. A. Hachtel, A. Hu, R. C. Pooser, R. F. Haglund, and B. J. Lawrie, *Phys. Rev. B* **97**, 081404(R) (2018).
  - [31] P. L. Knight and P. W. Milonni, *Phys. Rep.* **66**, 21 (1980).
  - [32] D. F. Walls and G. J. Milburn, *Quantum Optics* (Springer, Berlin, 1994).
  - [33] M. O. Scully and M. S. Zubairy, *Quantum Optics* (Cambridge University Press, Cambridge, 1997).
  - [34] G. S. Agarwal, *Quantum Optics* (Cambridge University Press, Cambridge, 2012).
  - [35] H. J. Carmichael and D. F. Walls, *J. Phys. B* **9**, 1199 (1976).
  - [36] H. J. Kimble and L. Mandel, *Phys. Rev. A* **13**, 2123 (1976).
  - [37] H. J. Kimble, M. Dagenais, and L. Mandel, *Phys. Rev. Lett.* **39**, 691 (1977).
  - [38] F. Diedrich and H. Walther, *Phys. Rev. Lett.* **58**, 203 (1987).
  - [39] Th. Basché, W. E. Moerner, M. Orrit, and H. Talon, *Phys. Rev. Lett.* **69**, 1516 (1992).
  - [40] L. Fleury, J.-M. Segura, G. Zumofen, B. Hecht, and U. P. Wild, *Phys. Rev. Lett.* **84**, 1148 (2000).
  - [41] P. Michler, A. Imamoglu, M. D. Mason, P. J. Carson, G. F. Strouse, and S. K. Buratto, *Nature (London)* **406**, 968 (2000).
  - [42] P. Michler, A. Kiraz, C. Becher, W. V. Schoenfeld, P. M. Petroff, L. Zhang, E. Hu, and A. Imamoglu, *Science* **290**, 2282 (2000).
  - [43] C. Santori, M. Pelton, G. Solomon, Y. Dale, and Y. Yamamoto, *Phys. Rev. Lett.* **86**, 1502 (2001).
  - [44] I. Thanopoulos, E. Paspalakis, and V. Yannopapas, *J. Phys. Chem. C* **115**, 4370 (2011).
  - [45] V. Yannopapas, E. Paspalakis, and N. V. Vitanov, *Phys. Rev. Lett.* **103**, 063602 (2009).
  - [46] I. Thanopoulos, E. Paspalakis, and V. Yannopapas, *Phys. Rev. B* **85**, 035111 (2012).
  - [47] S. Evangelou, V. Yannopapas, and E. Paspalakis, *Phys. Rev. A* **86**, 053811 (2012).
  - [48] V. Yannopapas, *J. Opt. Soc. Am. B* **31**, 631 (2014).
  - [49] N. Stefanou, V. Yannopapas, and A. Modinos, *Comput. Phys. Commun.* **113**, 49 (1998); **132**, 189 (2000).
  - [50] V. Yannopapas, A. Modinos, and N. Stefanou, *Opt. Quantum Electron.* **34**, 227 (2002).
  - [51] R. Sainidou, N. Stefanou, and A. Modinos, *Phys. Rev. B* **69**, 064301 (2004).
  - [52] B. Huttner and S. M. Barnett, *Phys. Rev. A* **46**, 4306 (1992).
  - [53] H. T. Dung, L. Knöll, and D.-G. Welsch, *Phys. Rev. A* **57**, 3931 (1998).